

Plasma-Driven Atomic-Scale Tuning of Metal Halide Perovskite Surfaces: Rationale and Photovoltaic Application

Alberto Perrotta, Sara Covella, Francesca Russo, Fabio Palumbo, Antonella Milella,*
Vincenza Armenise, Francesco Fracassi, Aurora Rizzo, Silvia Colella,* Waldemar Kaiser,*
Asma A. Allothman, Edoardo Mosconi, Filippo De Angelis, and Andrea Listorti

The effective defect passivation of metal halide perovskite (MHP) surfaces is a key strategy to simultaneously tackle MHP solar cell performances enhancement and their stability under operative conditions. Plasma-based dry processing is an established methodology for the modification of materials surfaces as it does not present the disadvantages often associated with wet treatments. This is becoming a fine tool to reach precise atomic-scale engineering of the MHP surfaces. Herein is reported a comprehensive picture of the interaction between different plasma chemistries and MHP thin films. The impact of Ar, H₂, N₂, and O₂ low-pressure plasmas on MHP optochemical properties and morphology is correlated with the performance of photovoltaic devices and rationalized by density functional theory calculations. Strong morphological modifications and selective removal of the uppermost methylammonium moieties are deemed responsible for nonradiative surface defects suppression and higher solar cell performances. Ellipsometry and X-ray photoelectron spectroscopies shine light on the subtle modifications induced by the different plasma environments, paving the way for the more effective engineering of plasma-based (deposition) processing. Notably, for O₂ plasma treatment, deep-state traps induced by the formation of IO₄⁻ species are demonstrated and rationalized, highlighting the challenges in optimizing O₂ plasma-based solutions for MHP-based devices.


1. Introduction

Metal halide perovskites (MHP) stand out as one of the most promising materials, steering the progress of various tech-applications, in particular photovoltaics (PV), light-emitting diodes, photodetectors, and recently photo(electro)chemical devices. Their success is largely due to their straightforward processing which comes along with outstanding optoelectronic qualities, such as high absorption coefficient, tunable bandgap energy, and high charge carrier mobility.^[1–5] Particularly in PV such properties increased the power conversion efficiency (PCE) of perovskite-based solar cells (PSCs) to over 25.7%.^[6] Herein, one of the major challenges facing the commercialization of PSCs is the material instability under working conditions, being strongly related to their processing and final quality. Degradation mainly originates at surfaces, especially under operative conditions; thus, chemical engineering of MHP surfaces has been targeted as a possible means to tackle these problems.^[7–9]

Additionally, surface modification can reduce the defect density, improve interfacial contact, and promote energy-level alignment, contributing to improve both device performance and stability.

A. Perrotta, F. Palumbo, F. Fracassi, S. Colella
CNR NANOTEC – Istituto di Nanotecnologia – c/o Dipartimento di
Chimica
Università degli Studi di Bari “Aldo Moro”
70126 Bari, Italy
E-mail: silvia.colella@nanotec.cnr.it

S. Covella
Dipartimento di Chimica, Biologia e Biotecnologie
Università degli Studi di Perugia
06123 Perugia, Italy

 The ORCID identification number(s) for the author(s) of this article can be found under <https://doi.org/10.1002/solr.202300345>.

© 2023 The Authors. Solar RRL published by Wiley-VCH GmbH. This is an open access article under the terms of the Creative Commons Attribution License, which permits use, distribution and reproduction in any medium, provided the original work is properly cited.

DOI: 10.1002/solr.202300345

F. Russo, A. Milella, V. Armenise, F. Fracassi, A. Listorti
Dipartimento di Chimica
Università degli Studi di Bari “Aldo Moro”
70126 Bari, Italy
E-mail: antonella.milella@uniba.it

F. Russo
Dipartimento di Ingegneria Elettrica e dell’Informazione
Politecnico di Bari
70126 Bari, Italy

A. Rizzo, A. Listorti
CNR NANOTEC – Istituto di Nanotecnologia
73100 Lecce, Italy

W. Kaiser, E. Mosconi, F. De Angelis
Computational Laboratory for Hybrid/Organic Photovoltaics (CLHYO)
Istituto CNR di Scienze e Tecnologie Chimiche “Giulio Natta” (CNR-
SCITEC)
06123 Perugia, Italy
E-mail: waldemar.kaiser@scitec.cnr.it

While a plethora of wet chemistry approaches have been applied to tailor MHP surface stability,^[10–15] dry postprocessing techniques^[16–19] have been so far largely overlooked, despite the advantages these would bring in terms of industrial-level utilization as well as compatibility with the perovskite layer. More specifically, the nonequilibrium plasma treatment of MHPs is still at its infancy. One of its main advantages is the strictly superficial modification mechanism,^[20,21] retaining the MHP bulk properties and the decoupling of material synthesis, processing, and the surface optimization. Other key advantages of plasma treatments are their flexibility, the easy and controllable processing, and the dry and environmentally friendly nature, limiting pollution and chemical effluents that are largely employed in solution-based techniques. Both nonequilibrium low-pressure (LP) or atmospheric-pressure (AP) plasmas have been applied on MHP surface to improve their stability and enhance the device performance. When a surface is exposed to a plasma, numerous plasma–surface interactions can occur. Common interactions include not only adsorption processes, but also desorption steps, insertion reactions into strained bonds, photoinduced reactions, and processes either assisted or controlled by (positively charged) ion species. Usually, since the surface treatments are based on the use of nonequilibrium plasmas (i.e., cold plasmas), thermal effects on the surface of materials can be neglected by selecting the appropriate experimental conditions, as higher pressures (>100 mTorr) and low input powers.^[22]

Next to the plasma treatment itself, plasma processing comprises several dry deposition techniques, such as plasma-enhanced chemical vapor deposition (PECVD), plasma-enhanced atomic layer deposition (ALD), and plasma polymerization, which are largely adopted in the fabrication of PV devices.^[23–26]

In this context, only a handful of reports has dealt with the interaction between plasma and perovskite materials. Most of these studies report on the use of AP plasma as a tool to modify the surface properties, including morphology, chemistry, photoluminescence (PL), and the consequent device performances. Masoud et al. reported on the effect of ambient air plasma treatment on the properties of methylammonium lead halide perovskite films.^[27] A remarkable change in the energy bands, depending on treatment time, was observed. Short plasma treatments (≤ 5 s) led to a widening of the bandgap, probably due to a higher carrier concentration, while longer plasma treatment (>5 s) led to narrowing of the bandgap. In addition, short plasma treatments were able to increase perovskite crystallinity, as proved by X-ray diffraction (XRD) measurements, while a long

treatment time created a nonhomogeneous etched surface. A slight increase in the energy gap was also observed upon the interaction between a methylammonium lead iodide MAPbI₃ film and a portable plasma source, directly operated in a nitrogen glovebox.^[28] This change was attributed both to the modification of the surface chemistry (change in Pb and I concentration) and the disruption of the vacancy equilibrium on the surface. Furthermore, the device performance was tested and an increase of 1.43% in the PCE was observed.

Similar was the result of Tsai et al., who obtained a 52.5% improvement in the PCE in a phenyl-C61-butyric-acid-methyl-ester (PCBM)-based device after the interaction between the perovskite surface and a portable atmospheric-pressure dielectric barrier discharge, used inside a glovebox. In this case, the enhancement was attributed to the reduction of nitrogen and carbon contents, as confirmed by X-ray photoelectron spectroscopy (XPS) measurements, suggesting the formation of a lead-rich surface successively passivated by PCBM.^[29]

Pioneering the above mentioned is the work of Xiao et al., who proposed the use of argon plasma as a tool to remove methylammonium and I ions to leave a lead-rich perovskite surface, which could be better passivated by electron transport materials, as fullerene derivatives.^[30] XPS measurements indicated a reduction of the carbon, nitrogen, and iodine superficial content and the formation of metallic lead. Furthermore, using the thermal admittance spectroscopy, the Ar plasma-treated perovskite showed a lower trap density of states, which could probably help fullerenes to diffuse into the grain boundaries (GB), to passivate the shallow trap located at the GB, as well as passivate the deep trap at the surface. The resulting device showed an improved PCE of 18.4%, higher than the 16.3% of the untreated device. A different plasma was used by Kim et al, namely, an atmospheric hydrogen plasma, to etch MAPbI₃ films. In this study, the plasma was not used to enhance the surface properties or for passivating purposes, but only to etch the perovskite surface, as an effective and economic way to pattern the material. Plasma treatment time shorter than 180 s was found to etch the surface without altering the surface chemistry, while a longer treatment time led to cluster formation and film decomposition.^[31] Hydrogen was also used as an alternative method to thermal annealing for crystallization of MHP films.^[32]

Different from the above-mentioned examples, Armenise et al. used plasma to deposit a fluorocarbon coating on MAPbI₃ perovskite. The treatment increased the film resistance to moisture, thanks to the hydrophobic character of the fluorinated polymer.^[33]

Besides the reported literature, which somehow represent a scattered and often contradictory collection of insights, a comprehensive picture on the effect of plasma treatments upon perovskite surfaces has not been drawn, leaving open many interesting research fronts. For these reasons, we investigate the effect of plasma treatments, using Ar, N₂, H₂, and O₂, on the most common and explored MAPbI₃ perovskite layer, in terms of surface morphology and chemistry, as well as modifications of the optoelectronic properties, using experimental characterization and first-principal calculations. Photovoltaic devices were fabricated including the differently modified layers as a comprehensive diagnostic tool of the surface properties. The ones including the Ar- and H₂- treated perovskite films are

A. A. Allothman, E. Mosconi
Department of Chemistry
College of Science
King Saud University
Riyadh 11495, Kingdom of Saudi Arabia

F. De Angelis
Department of Chemistry, Biology and Biotechnology
University of Perugia and INSTM
06123 Perugia, Italy

F. De Angelis
SKKU Institute of Energy Science and Technology (SIEST) Sungkyunkwan
University
Suwon 440-746, Korea

the ones that sowed better device performances. Worsening of photovoltaic performances was instead observed for the N_2 and O_2 plasma-treated devices. Our results provide a detailed understanding of the plasma-induced surface modifications, serving as a base for the development and engineering of plasma-controlled MHP surfaces for efficient optoelectronic devices.

2. Results and Discussion

$MAPbI_3$ perovskite films, with a thickness of about 430 ± 10 nm, were exposed to LP plasma treatments. Four different gases were tested, that is, Ar, H_2 , N_2 , and O_2 , and the treatment time was varied from a minimum of 2 to a maximum of 30 s, depending on the incidence of the specific gas. Ar plasma was chosen to solely explore the ion bombardment effect, excluding the chemical modification of the surface due to the absence of chemically active species in this plasma. H_2 plasma was chosen to explore the effect that a reducing environment can have on the perovskite surface. N_2 plasma was explored because of its potentially good affinity with a perovskite as $MAPbI_3$, containing nitrogen atoms. The positive effect of nitrogen soaking into perovskite lattice

discontinuity^[34] represents an interesting preliminary observation to our investigations, suggesting a beneficial nitrogen effect on the perovskite surface, although the treatment conditions differ from the ones of this study. Furthermore, both H_2 and N_2 plasmas are largely employed in plasma-enhanced ALD and CVD techniques; therefore, the exploration of their interaction with perovskite surfaces can help to tailor and optimize the application of the deposition methods to apply buffer layers and/or passivate surface defects to improve photovoltaic devices outcome.

The O_2 plasma was also explored, starting from the interesting oxidative passivation of perovskite surface observed by Goddig et al.,^[14] even though some works report that an oxygen plasma environment can heavily modify the surface and might not be the best solution in applications such as plasma-enhanced ALD.^[23]

2.1. Plasma-Induced Morphological Modifications and Films Implementation in PV Devices

Scanning electron microscopy (SEM) images up to 10 s of treatment are reported in **Figure 1**, while the 30 s treatment, showing

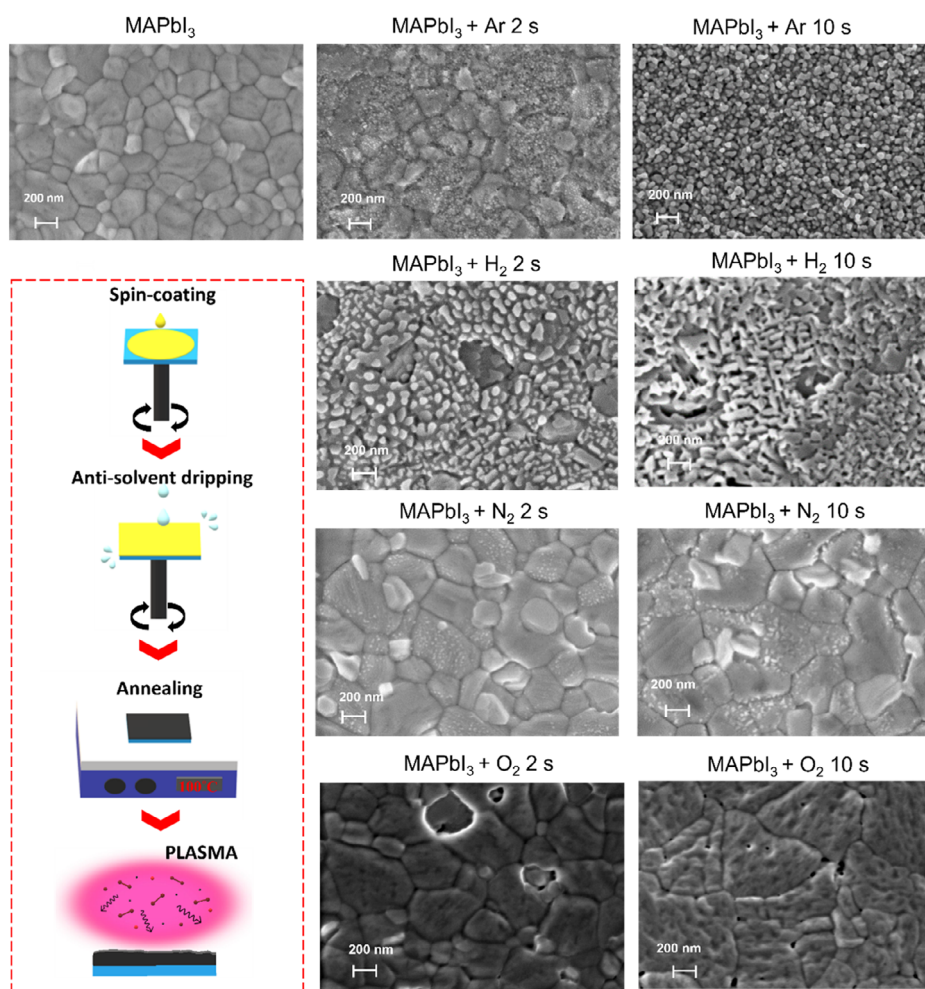


Figure 1. Schematization of the film processing and SEM images of pristine $MAPbI_3$ and of samples after 2 and 10 s of plasma treatment with different gases.

for all gases a significantly damaged surface, is shown in Figure S1, Supporting Information.

All gases impart strong morphological changes on the surface of the perovskite. We can neglect that these changes are due to thermal modifications, since the characteristics of the adopted plasma (type of reactor, RF input power and pressure) are usually associated with a gas temperature not higher than 50–60 °C, as aforementioned. Even after 2 s of Ar plasma, the GBs are no longer sharp as the ones of the pristine sample. A longer treatment time even leads to the formation of nanosized domains and the complete disappearance of the perovskite large grains. We ascribed these morphological changes to the solo bombardment effect induced on the surface by the Ar ions, as, due to the nature of the plasma species involved in the process, we can exclude chemical changes during the plasma step due to the nature of the plasma species involved in the process. SEM images for H₂ plasma also show an evident morphological change already after 2 s of treatment,^[23] with a significant reduction of the grain size. Similar results were reported by Khachatryan et al. in exploring the etching effect of atmospheric pressure hydrogen plasma on MAPbI₃ films.^[35] For all H₂ plasma-treated films, the grains cannot be distinguished anymore, indicating the intense effect of hydrogen plasma on the perovskite surface.

N₂ plasma, on the other hand, does not drastically affect the surface morphology. Perovskite grains are still well defined after 10 s of treatment, while an evident modification is detectable only for the sample treated for 30 s (Figure S1, Supporting Information). Interestingly, for the samples treated for 2 and 10 s, only some crystal grains show brighter spots on their surface, while others seem not affected by the plasma. It can be speculated that certain crystal facets are more vulnerable to the N₂ plasma environment than others, as reported for moisture-induced degradation on FAPbI₃ films.^[36] In fact, C. Ma et al. observed that the (100) crystal facets of FAPbI₃ films were substantially more vulnerable to moisture-induced degradation than the (111) facets, which instead showed a better thermodynamic stability against surface interaction with water molecules. This could be part of the N₂/perovskite interaction complexity that we observed, as randomly oriented surface distribution would differ from film to film.

O₂ has a peculiar behavior. After 2 s of treatments, the surface seems to be only selectively damaged, while the grains have a melted appearance for the 10 s treatment. Homogeneously distributed darker regions are formed after the treatment, pointing out at the local removal of surface material.

A stability test was carried out to understand if the plasma treatment can negatively affect the perovskite resistance to moisture. Therefore, pristine and plasma-treated MAPbI₃ films were exposed to open air (humidity in the range of 23–38%, at a temperature of about 21 °C) for 4 weeks and UV absorption spectra were recorded weekly. The latter are reported in Figure S2, Supporting Information. No relevant differences were observed, not even for the most aggressive treatments (i.e., in Ar and H₂ plasmas), proving that the plasma treatments do not significantly accelerate the ambient-induced degradation of the perovskite layers.

Plasma-treated perovskite films and, for comparison, untreated ones were implemented in photovoltaic devices in an inverted p–i–n architecture, according to the structure

reported in Figure 2a and detailed in Experimental Section in Supporting Information.

For the fabrication of devices, based on the morphological results, only the 2 s treatment was considered. Longer plasma exposures were excluded due to the significant impact on the film morphologies. We particularly observed an increased surface roughness, likely negatively affecting the device interfaces (see SEM in Figure 1 and S1, Supporting Information). Best-performing devices *J*–*V* curves are reported in Figure 2b, while the average values and the relative standard deviation of the solar cells parameters are reported in Figure 2c, taking into account the variables affecting the device reproducibility.

We compared the average PCE value of the device containing the Ar plasma-treated film, 17.0 ± 1.3%, to the performance of the control (15.7 ± 1.0%), detecting a slight, although statistically significant, increase.

The device with the H₂ plasma-treated MHP layer shows same performance as the control one (15.6 ± 1.5%), proving the benign nature of the H₂ plasma, despite the deep morphological changes.

It is worth noticing that in both cases the devices show an overall improved fill factor (FF) with respect to the pristine, attributed to the passivation of defects in the absorber material.

N₂ plasma-treated perovskite films result in reduced device performance, showing a PCE of 8.8 ± 0.7% and almost half of the extracted current. Finally, in the O₂ plasma-treated device, the current almost completely vanishes with PCE close to zero. Although the morphological changes are not relevant for the latter two gases, the reason behind the worsening of performances is likely caused by implications of the surface modification on the interface properties in the device.

2.2. Optical Properties of Plasma-Modified Films

The strictly superficial modification of the perovskite layer is proved by the optical properties retrieved from UV–vis analysis (Figure S3, Supporting Information). All the UV–vis spectra exhibit the same features, with the absorption onset at about 780 nm, typical of MAPbI₃ perovskite.^[33] The unchanged energy gap values derived from the Tauc plots for the pristine and 30 s plasma-treated samples are reported in Figure S4, Supporting Information.

The absorption coefficient was obtained through spectroscopic ellipsometry measurements. Importantly, the adopted model, described in Experimental Section, allowed us to separate the optical properties of the bulk material from the ones of the surface layer, therefore allowing the isolation of the effect of the plasma. For the Ar plasma treatment, the trends of the absorption coefficient for the bulk material of the pristine and the plasma-treated samples are reported in Figure S5, Supporting Information. The absorption onset at around 780 nm well agrees with the UV–vis spectra of Figure S3, Supporting Information, confirming the robustness of the model. Both pristine and plasma-treated samples show similar trends, confirming that all plasma treatments affect only the surface, but not the bulk properties. The trends of the absorption coefficient for the surface layer of all gases are shown in Figure 3a–d. For Ar plasma, the absorption spectra and *n* and *k* as a function of the

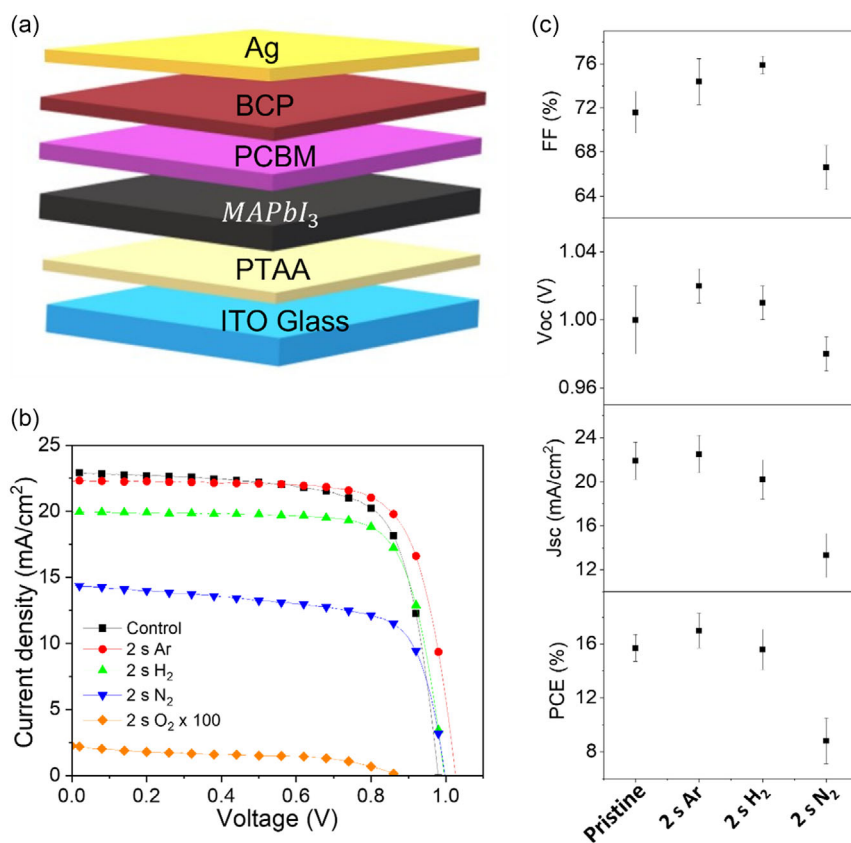


Figure 2. a) Device architecture; b) $J - V$ curves of solar devices; c) device parameters and statistics for the reference and the plasma-treated films (oxygen-treated samples have been removed for clarity).

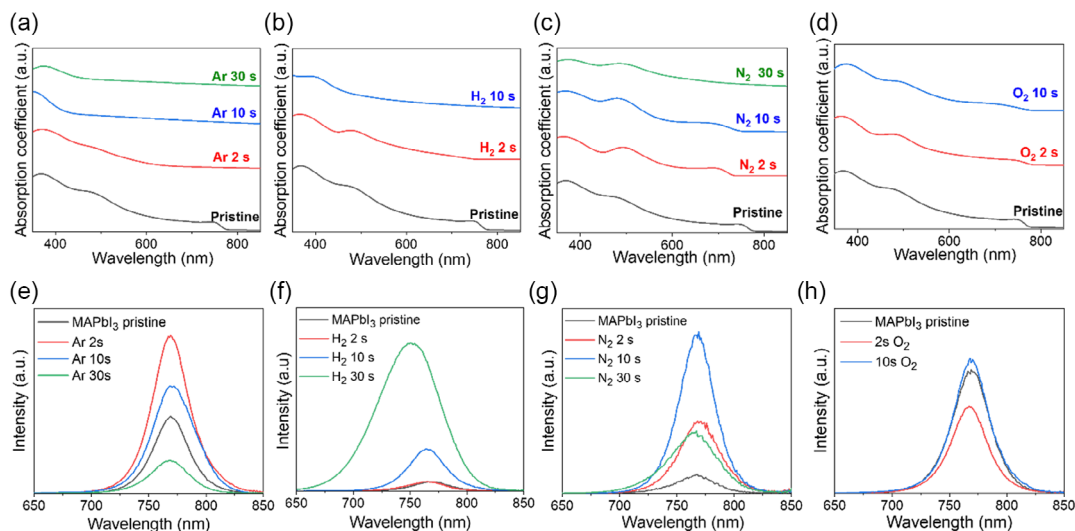


Figure 3. Ellipsometry-derived surface layer absorption coefficient and PL spectra of pristine MAPbI₃ and of samples after a,e) Ar; b,f) H₂; c,g) N₂; and d,h) O₂ plasma treatment.

wavelength of the pristine MAPbI₃ layer show the critical points at $E_0 = 1.55$ eV, $E_1 = 2.5$ eV, and $E_2 = 3.4$ eV, in agreement with ellipsometry analyses reported for MAPbI₃.^[37,38] The surface layers have a lower absorption due to the presence of the modeled

voids; however, they show the same absorption peaks of the modeled bulk layers. Due to the grain dimension close to the wavelength adopted in the ellipsometry analysis, the void fraction in the EMA model was left unbound during modeling to avoid

artefacts.^[37] Upon application of the first Ar plasma treatment of 2 s, a below-bandgap absorption arises, together with a decrease in the absorption relative to the E1 peak. For a longer treatment time, the below-bandgap absorption increases and the E1 is further suppressed, together with a decrease of the E2 peak. The E0 absorption is still present, but dramatically reduced, and this is attributed to the grain size reduction upon plasma exposure, together with an increase in roughness, pointing out the sensitivity of the model in identifying surface modifications. For clarity, in Figure S6, Supporting Information, a zooming on the E0 peaks for the Ar treatment has been reported for all samples, in which the absorption onset can be clearly observed. Moreover, the model suggests an increase of the void fraction of the surface layer with the treatment time, going from 22% to 33%, in agreement with SEM analysis.

The absorption coefficient plots for the surface layer of the H₂ plasma-treated films (Figure 3b) are shown only up to 10 s of plasma treatment, since the substantial modification of the sample treated for 30 s, as confirmed by SEM images, made these data really complex to model. The absorption spectra show similar features discussed for the Ar plasma treatment. Sub-bandgap absorption arises already after 2 s, together with a decrease in the absorption relative to the E1 and E2 peaks. The dramatic reduction of the E0 absorption is attributed also in this case to the increase in surface roughness and reduced grain size.

In the case of N₂ plasma-treated films (Figure 3c), instead, the intensity of the E0, E1, and E2 obtained through ellipsometry measurements remains almost unchanged for 2 and 10 s, in agreement with the little surface modifications observed with SEM analysis. However, a slight blueshift in the bandgap can be observed for the plasma-treated films with respect to the pristine sample, presumably ascribable to the chemical changes imparted by the N₂ plasma. The sample treated for 30 s shows an abrupt reduction of the E0 absorption because of the reduced grains and the increase in surface roughness, as monitored with SEM analysis and an increase of the voids fraction (from 26% of the pristine sample to 48%).

Ellipsometry gave a different response for O₂ plasma-treated samples, as reported in Figure 3d. The void fraction tends to decrease as a function of the plasma exposure time (from 29% to 17% after 10 s of treatment), pointing at a densification of the surface layer. Furthermore, the refractive index of the modeled surface layer was found comparable (2.33 of the O₂ plasma treated vs 2.37 of the pristine MHP surface, accounting for the void fraction) throughout the whole range of the explored wavelength. No sub-bandgap absorption was modeled, indicating a lower roughness of the perovskite surface, as also retrieved from the SEM analysis. Finally, the critical points retain their position and intensity, except for the bandgap which undergoes a widening and a redshift upon the first exposure to the oxygen plasma, without significant changes as a function of the exposure time. We speculate the formation of a PbO layer, which could shield the perovskite surface from further plasma damage, differently from the other treatments which etch and dramatically modify the material surface.

Optical analysis was completed by PL investigation to provide information about defects and charge-trapping states within the perovskite film. The steady-state PL spectra reported in Figure 3e show that Ar plasma treatment raises the intensity of steady-state

PL emission. All treated samples, except the 30 s one, show a more intense PL emission than the pristine material, with the highest value after processing of only 2 s. The increased emission suggests efficient reduction of electronically active surface defects. In contrast, a longer treatment time show a monotonic reduction of the emission intensity, in line with the deterioration of the MHP surface.

H₂-treated films show a continuous improvement of PL emission with time (Figure 3f). Peculiar is the sample treated with H₂ plasma for 30 s, showing a much higher emission and a blueshift of about 20 nm, which is usually associated with suppressed non-radiative recombination due to reduced surface defects.^[39]

The trend in PL with N₂ plasma treatment time (Figure 3g) is not reproducible over different samples. As shown in Figure S7, Supporting Information, a decrease of PL emission was observed after the same N₂ plasma treatment of a different batch. This suggests a nontrivial and complex interaction between the perovskite and N₂ plasma. Finally, O₂ plasma-treated MHPs show an unclear trend of the PL emission as a function of the treatment time, however significantly worsening the PL intensity.

2.3. Chemical Characterization

XPS analysis were carried out to gain more insight into the surface chemical modifications upon plasma treatment (Figure S8, Supporting Information).

The atomic concentrations of the functional groups derived from the high-resolution XPS peaks of carbon, nitrogen, lead, and iodine are reported in Figure 4, as a function of the plasma treatment time. The atomic concentrations of each element (C1s, 13d_{5/2}, Pb4f_{7/2}, N1s, O1s) are instead reported in Table S1, Supporting Information, for each plasma treatment, as a function of the treatment time.

The superficial atomic concentration of nitrogen tends to decrease for all gases, whereas carbon decreases in all cases except for N₂, as will be discussed later in the text. The reduction of nitrogen as a function of the treatment time is compatible with the removal of the methylammonium cation.

For Ar plasma (Figure 4a,b), oxidized carbon is formed and increases as a function of the plasma treatment, together with an increased oxygen concentration. C–O (286.0 eV) tends to decrease in favor of more carbonyl (287.1 eV) and carboxyl (288.8 eV) moieties at the surface level. Their formation is due to the exposure of the perovskite layers to air after the treatment, as the Ar plasma alone cannot introduce additional chemical moieties at the perovskite surface but can only contribute, via ion bombardment, to the aforementioned morphological changes. For a longer treatment time, the formation of lead oxide and hydroxide was found, as retrieved from the components at 529.5 and 531.5 eV, respectively, of the high-resolution O1s spectrum, reported in Figure S9, Supporting Information. These data suggest that, after the removal of methylammonium cations caused by the ion bombardment, the inorganic surface is further activated, leading to the reaction of the exposed lead-rich surface with oxygen-containing air species. [I]-to-[Pb(II)] ratio, calculated from the high resolution peaks at 619.3 eV (iodine) and 138.4 eV (lead(II)), (see Figure S10, Supporting Information), decreases from 2.6 to 2.4, showing a general decrease of iodine. Further

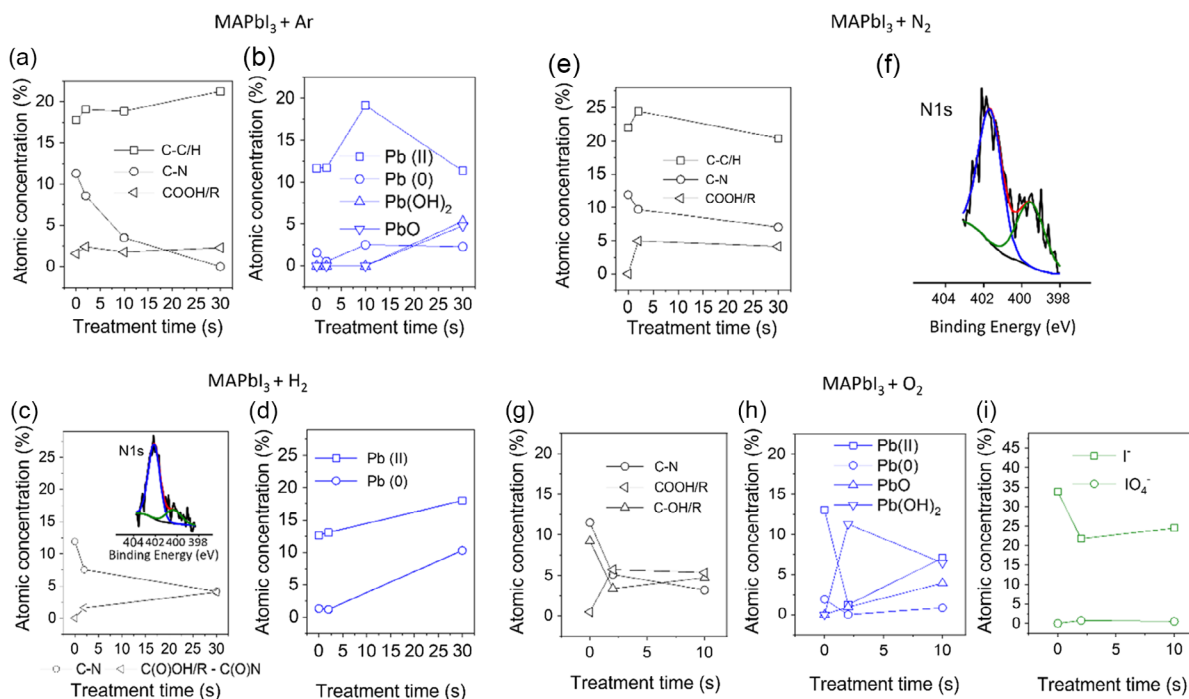


Figure 4. XPS atomic concentration as a function of plasma treatment time for a,b) Ar; c,d) H₂; e,f) N₂; g-i) O₂ plasma treatment.

studies in an inert environment are ongoing to distinguish between the effects of the ion bombardment and the chemical modification in air following the surface activation.

While for the Ar plasma treatment, an interplay between surface activation and air exposure accounts for the surface chemical modification; for the other gases, additional chemical functionalities are measured which are also induced by the reactive plasma chemistry during treatment. In the H₂-treated samples (Figure 4c,d), an increase of Pb(II) (138.5 eV) can be observed after 30 s of treatment caused by the reducing nature of H₂ plasma.

In the H₂-treated samples (Figure 4c,d), an increase of Pb(II) (138.5 eV) can be observed after 30 s of treatment caused by the reducing nature of H₂ plasma in this case with simultaneous increase of Pb(0) (136.8 eV). The formation of Pb(0), together with the blueshift in UV-vis, was further observed by Jin et al. by exposing a perovskite surface-to-electron bombardment.^[39] The blueshift was attributed to the exposure of a fresh surface with suppressed defects^[40] after the knock-on effect induced by electrons. In a similar way, we observed a blueshift in a reducing environment, even though, in our case, the plasma dynamics and induced morphological changes make the deduction more complex.

In addition, unlike Ar plasma, H₂ plasma treatment determines a reduction of the hydrocarbon component (284.8 eV), while as for the Ar plasma, there is an increase in surface C-O and carboxyl moieties. Furthermore, after 2 s of treatment, a new peak appears in the high-resolution N1s spectrum at low binding energy (400.3 eV), which can be attributed to an additional amide group. This counterintuitive oxidation of the ammine can be explained not as the effect of the direct

interaction between the H₂ plasma and perovskite surface, but more likely because of the interaction between the activated perovskite surface and the external ambient. Exposure of the activated surfaces in a controlled environment would help to isolate the effect of H₂ plasma alone. The [I]-to-[Pb(II)] ratio decreases from 2.7 to 1.9, confirming a general decrease of the iodine content also in this case.

Different from Ar and H₂ plasma, the N₂-treated samples show a slight increase in surface carbon, originating from the external ambient, as shown in Figure 4e,f. Most likely, the increase of the carbon moieties plays a crucial role both for PL emission and for the device performances.

In addition, a slight reduction of the C-N component and an increase of C-O and carboxyl moieties can be observed. After 30 s of treatment, a new peak appears at low binding energy (399.5 eV), as shown in the Figure 3e. This new functionality can be attributed to an additional amine group formed after exposure of the perovskite to the N₂ plasma, which may originate from the methylammonium ion decomposition or by the introduction of N-containing moieties on the adventitious carbon. Comparable to the other gases, [I]-to-[Pb(II)] ratio reduces from 2.7 to 1.9.

O₂ plasma causes a decrease in carbon, nitrogen, and iodine with simultaneous increase in lead and oxygen surface concentration. A significant increase of carbonyl and carboxyl moieties can be observed after 10 s of treatment (Figure 4g-i). Notably, we observe substantial increase in Pb(OH)₂, PbO, and IO₄⁻ (624 eV) concentration. These moieties can form an insulating surface layer, which can hamper interfacial electron transfer from the perovskite to the PCBM electron transport layer, explaining the deterioration of the device performance. The [I]-to-[Pb(II)]

ratio decreases from 2.6 to 0.7 after 10 s of treatment, pointing at a profound modification of the surface chemical composition. The formation of an insulating denser PbO layer on the surface of the MHP is also in agreement with SEM images (Figure 1) and ellipsometry (Figure 3d).

2.4. Theoretical Rationalization

Short-time surface treatment with Ar plasma showed the removal MAI from the surface, leaving partially PbI₂-terminated grains. Density-functional theory (DFT) calculations predict adsorption energies of -0.69 eV for acetic acid and of -0.86 eV for formamide on a MAPbI₃ surface, representative for the experimentally observed carboxyl and carbonyl moieties (see Table S2 and Figure S11, Supporting Information), respectively. Both species may passivate undercoordinated Pb surface atoms via formation of Pb–O bonds without introducing electronic states in the bandgap (see Figure S11, Supporting Information). The surface passivation likely causes the enhanced PL (Figure 3a) and improves the V_{oc} and FF (Figure 2a) at 2 s Ar plasma treatment. On longer timescales, hydroxide ions may accelerate surface degradation by deprotonation of the MA cation.^[41] We further expect a strong increase in defect density due to the reduction of grain size after 10 s, see Figure 1, as grain surfaces and GBs are sources of halide defects which may act as trap states.^[42–44]

H₂ plasma results in comparable changes such as for Ar plasma. In addition, H₂ plasma treatment reduces Pb(II) to metallic Pb(0), which, after 30 s, shows large structural voids (Figure S1, Supporting Information) as previously reported by Manna and coworkers.^[45]

N₂ plasma introduces carboxyl moieties and additional amine groups (see Figure 4e,f). We computed adsorption energies on PbI₂-terminated surfaces, matching the experimentally observed surface composition, for methylamine, dimethylamine, and trimethylamine of -0.85 , -0.92 , and -0.89 eV, respectively (see Table S2, Supporting Information). As for the acetic acid, all considered amines do not introduce gap states and passivate the undercoordinated Pb atoms via formation of strong Pb–N bonds, yielding the experimentally observed PL increase (Figure 3g). The increased number of methyl groups, however, may weaken the binding of the perovskite with the transport layers, likely resulting in an increased surface resistance and consequently, as experimentally observed (Figure 2a), reduced J_{sc} and FF.

The increase in Pb(OH)₂ and PbO upon O₂ plasma treatment has also been observed in previous photo-oxidation experiments of MAPbI₃,^[46–48] likely mediated through the light-induced formation of superoxide species.^[49,50] Thus, we may rationalize the formation of given lead oxide species due to electronic excitations of the O₂ molecules in the plasma environment. The increase of these moieties can be responsible for the formation of an insulating layer on top of the perovskite surface, which hampers the electron transfer to the electron transport layer in PSCs.^[46,51] To the best of our knowledge, periodate, IO₄[−], has not been reported in perovskite degradation studies. We performed DFT calculations to investigate IO₄[−] formation and its impact on the electronic properties of MAPbI₃. The oxidation of I[−] at the MAI-terminated MAPbI₃ surface to IO₄[−] consumes two oxygen molecules, following Equation (1).

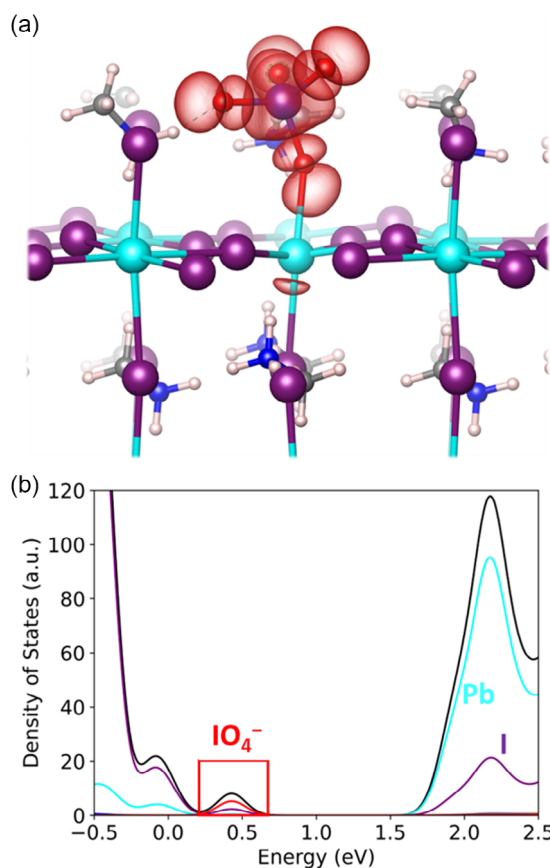


Figure 5. a) Visualization of unoccupied electronic state on surface IO₄[−]. The color code is as follows: purple, I; red, O; cyan, Pb; blue, N; grey, C; white, H; b) density of states of the MAI-terminated MAPbI₃ with IO₄[−].



The oxidation product bonds with an oxygen atom to the adjacent Pb ion, resulting in a Pb–O–I[−] bond network, see Figure 5a. Our calculations suggest that Equation (1) is endothermic with calculated energy difference of $\Delta E = +0.29$ eV ($+0.38$ eV on a PbI₂-terminated surface, see Figure S12, Supporting Information), while previous studies reported an exothermic nature of IO₃[−] formation.^[52] The observation of IO₄[−] by XPS, Figure 4c, suggests that the aggressive plasma treatment is sufficient to activate the endothermic periodate formation, which otherwise may be ruled out under standard fabrication conditions. Interestingly, surface IO₄[−] introduces electronic states in the bandgap at 0.4 eV above the valence band maximum of MAPbI₃, see Figure 5b. Moreover, the assigned orbital is strongly localized on IO₄[−], see Figure 5a, which may consequently act as an electronic trap state and deteriorate the electronic performance of O₂ plasma-treated perovskite films.^[53–56]

3. Conclusion

In conclusion, the impact of various plasma treatments on MHP surface has been evaluated and rationalized. The different

plasma chemistries of the considered gases, Ar, N₂, H₂, and O₂, are found to differently affect the morphological, chemical, and optoelectronic properties of the perovskite films, as well as the performances of deriving MHP-based p–i–n solar cells. The conditions associated with a more aggressive environment toward perovskite surface (Ar and H₂ gasses), in terms of organic component removal and film etching, are also the ones that more positively impact the corresponding device performances. The removal of the superficial organic components helps to better passivate the photoactive layer when included in the device structure, likely due to an enhanced coupling with electron-extracting PCBM layer.

Another interesting aspect of the chemical modification induced by the plasmas is the in situ generation of chemical functionalities (e.g., amides, amines) that change the energetic landscape of the interfaces, as confirmed by modeling. We observe a general positive effect on the bandgap engineering with respect to PCBM. This positive effect is however counterbalanced by the surface activation, which, for mild plasma conditions, leads to the formation of an insulating layer likely deriving from the capture of environmental pollutants (N₂ gas). Noticeably, the controlled introduction of additional chemical functionalities at the perovskite surface, via plasma, opens novel possibilities for the MHP surface engineering as an alternative, less-invasive, and technologically mature route to classical wet chemistry.

Finally, a peculiar behavior is observed when O₂ plasma is applied: the introduction of insulating Pb(OH)₂, PbO, and periodate IO₄[−]. The electrical barrier generated by the formed compounds, in particular PbO, has a clear negative effect on the solar cell performances. This finding adds an important piece of information to the defect chemistry of perovskite materials: the oxidation of iodide resulting in periodate IO₄[−] is possible in O₂ plasma conditions and despite showing substantial positive formation energies has never been reported so far as degradation intermediate in MHP. This result extends beyond this work, as oxidative plasma environments are associated to several dry deposition techniques, such as PECVD, PEALD, and plasma polymerization, which are largely adopted in the fabrication of PV devices. Overall, our results underline the great potential of plasma-based treatment to passivate and functionalize the surface of MHPs; at the same time it raises the need for additional efforts in the engineering of the plasma conditions to minimize plasma damage and controlled surface modification.

Supporting Information

Supporting Information is available from the Wiley Online Library or from the author.

Acknowledgements

A.P. and S.C. contributed equally to this work. The authors thank S. Cosmai and D. Benedetti for the technical support. W.K., E.M., and F.D.A. acknowledge funding by the European Union. Views and opinions expressed are however those of the author(s) only and do not necessarily reflect those of the European Union or CINEA. Neither the European Union nor the granting authority can be held responsible for them. VALHALLA project has received funding from Horizon Europe Research and Innovation Action programme under grant agreement n°

101082176. This work was also supported by the MIUR project “ECOTEC – ECO-sustainable and intelligent fibers and fabrics for TEChnic clothing”, PON «R&I» 20142020, project N° ARS01_00951, CUP B66C18000300005. S.C. and E.M. acknowledge Project Ricerca@CNR PHOTOCAT (CUP B93C221000060006). This work was further funded by the European Union - NextGenerationEU under the Italian Ministry of University and Research (MUR) National Innovation Ecosystem grant ECS00000041 - VITALITY. F.D.A. acknowledges the Università degli Studi di Perugia and MUR for support within the project Vitality. E.M. and A.A.A. wish to thank the Distinguished Scientist Fellowship Program (DSFP) of King Saud University, Riyadh, Kingdom of Saudi Arabia.

Conflict of Interest

The authors declare no conflict of interest.

Data Availability Statement

The data that support the findings of this study are available from the corresponding author upon reasonable request.

Keywords

metal halide perovskites, photovoltaics, plasma processing, surface modifications

Received: May 9, 2023

Revised: June 26, 2023

Published online: July 20, 2023

- [1] A. Rajagopal, K. Yao, A. K. Y. Jen, *Adv. Mat.* **2018**, *30*, 1800455.
- [2] L. M. Herz, *ACS Energy Lett.* **2017**, *2*, 1539.
- [3] A. D. Wright, C. Verdi, R. L. Milot, G. E. Eperon, M. A. Pérez-Osorio, H. J. Snaith, F. Giustino, M. B. Johnston, L. M. Herz, *Nat. Commun.* **2016**, *7*, article no. 11755.
- [4] T. M. Brenner, D. A. Egger, L. Kronik, G. Hodes, D. Cahen, *Nat. Rev. Mat.* **2016**, *1*, article no. 15007.
- [5] H. Li, C. Cui, X. Xu, S. Bian, C. Ngoajampa, P. Ruankham, A. P. Jaroenjittchai, *Sol. Energy* **2020**, *212*, 48.
- [6] Q. Fu, A. K. Y. Jen, *Next Energy* **2023**, *1*, 100004.
- [7] S. Bera, A. Saha, S. Mondal, A. Biswas, S. Mallick, R. Chatterjee, S. Roy, *Mater. Adv.* **2022**, *3*, 5234.
- [8] P. Schulz, D. Cahen, A. Kahn, *Chem. Rev.* **2019**, *119*, 3349.
- [9] T. H. Han, S. Tan, J. Xue, L. Meng, J. W. Lee, Y. Yang, *Adv. Mater.* **2019**, *31*, 1803515.
- [10] Y. Shao, Z. Xiao, C. Bi, Y. Yuan, J. Huang, *Nat. Commun.* **2014**, *5*, 5784.
- [11] T. H. Han, S. Tan, J. Xue, L. Meng, J. W. Lee, Y. Yang, *Adv. Mater.* **2019**, *31*, 1803515.
- [12] D. W. Dequillettes, S. Koch, S. Burke, R. K. Paranjhi, A. J. Shropshire, M. E. Ziffer, D. S. Ginger, *ACS Energy Lett.* **2016**, *1*, 438.
- [13] Y. Chen, Q. Meng, Y. Xiao, X. Zhang, J. Sun, C. B. Han, H. Gao, Y. Zhang, Y. Lu, H. Yan, *ACS Appl. Mater. Interfaces* **2019**, *11*, 44101.
- [14] J. S. W. Godding, A. J. Ramadan, Y. H. Lin, K. Schutt, H. J. Snaith, B. Wenger, *Joule* **2019**, *3*, 2716.
- [15] X. Li, W. Zhang, X. Guo, C. Lu, J. Wei, J. Fang, *Science* **2022**, *375*, 434.
- [16] Q. Cao, S. Yang, Q. Gao, L. Lei, Y. Yu, J. Shao, Y. Liu, *ACS Appl. Mater. Interfaces* **2016**, *8*, 7854.

- [17] Z. Ren, A. Ng, Q. Shen, H. C. Gokkaya, J. Wang, L. Yang, W. K. Yiu, G. Bai, A. B. Djurišić, W. W. F. Leung, J. Hao, W. K. Chan, C. Surya, *Sci. Rep.* **2014**, *4*, 4.
- [18] A. Alberti, I. Deretzis, G. Mannino, E. Smecca, F. Giannazzo, A. Listorti, S. Colella, S. Masi, A. La Magna, *Adv. Energy Mater.* **2019**, *9*, 1803450.
- [19] B. Ding, J. Peng, Q. Q. Chu, S. Zhao, H. Shen, K. J. Weber, G. J. Yang, T. P. White, K. R. Catchpole, M. K. Nazeeruddin, P. J. Dyson, *Sol. RRL* **2021**, *5*, 2000729.
- [20] R. d'Agostino, P. Favia, F. Fracassi, *Plasma Processing of Polymers* (Ed: Kluwer Academic Publishers), NATO ASI Series, Dordrecht, The Netherlands; Boston, MA; London, UK **1996**.
- [21] H. F. Winters, R. P. H. Chang, C. J. Mogab, J. Evans, J. A. Thornton, H. Yasuda, *Mater. Sci. Eng.* **1985**, *70*, 53.
- [22] A. Agarwal, S. Rauf, K. Collins, *Plasma Sources Sci. Technol.* **2012**, *21*, 055012.
- [23] V. Zardetto, B. L. Williams, A. Perrotta, F. Di Giacomo, M. A. Verheijen, R. Andriessen, W. M. M. Kessels, M. Creatore, *Sustainable Energy Fuels* **2017**, *1*, 30.
- [24] D. Koushik, W. J. H. Verhees, Y. Kuang, S. Veenstra, D. Zhang, M. A. Verheijen, M. Creatore, R. E. I. Schropp, *Energy Environ. Sci.* **2017**, *10*, 91.
- [25] D. Koushik, F. Naziris, J. Melskens, A. Nusteling, V. Zardetto, H. Schut, W. M. M. Kessels, S. W. H. Eijt, M. Creatore, *J. Mater. Chem. C* **2019**, *7*, 5275.
- [26] J. M. Obrero-Perez, L. Contreras-Bernal, F. Nuñez-Galvez, J. Castillo-Seoane, K. Valadez-Villalobos, F. J. Aparicio, J. A. Anta, A. Borrás, J. R. Sanchez-Valencia, A. Barranco, *Adv. Energy Mater.* **2022**, *12*, 2200812.
- [27] M. Shekargoftar, J. Jurmanová, T. Homola, *Metals* **2019**, *9*, 991.
- [28] M. Shekargoftar, J. Pospisil, J. Dugáček, M. Weiter, T. Homola, *ACS Omega* **2020**, *5*, 18384.
- [29] J. H. Tsai, I. C. Cheng, C. C. Hsu, C. C. Chueh, J. Z. Chen, *Electrochim. Acta* **2019**, *293*, 056501.
- [30] X. Xiao, C. Bao, Y. Fang, J. Dai, B. R. Ecker, C. Wang, Y. Lin, S. Tang, Y. Liu, Y. Deng, X. Zheng, Y. Gao, X. C. Zeng, J. Huang, *Adv. Mater.* **2018**, *30*, 1705176.
- [31] H. P. Kim, M. Kim, K. B. Kim, H. Khachatryan, J. Jang, *Surf. Coat. Technol.* **2017**, *330*, 228.
- [32] M. Shekargoftar, T. Homola, *Plasma Chem. Plasma Process.* **2020**, *40*, 539.
- [33] V. Armenise, S. Colella, A. Milella, F. Palumbo, F. Fracassi, A. Listorti, *Energies* **2022**, *15*, 4512.
- [34] A. Alberti, I. Deretzis, G. Mannino, E. Smecca, F. Giannazzo, A. Listorti, S. Colella, S. Masi, A. la Magna, *Adv. Energy Mater.* **2019**, *9*, 1803450.
- [35] H. Khachatryan, H. P. Kim, S. N. Lee, H. K. Kim, M. Kim, K. B. Kim, J. Jang, *Mater. Sci. Semicond. Process.* **2018**, *75*, 1.
- [36] C. Ma, F. T. Eickemeyer, S.-H. Lee, D.-H. Kang, S. J. Kwon, M. Grätzel, N.-G. Park, *Science* **2023**, *379*, 173.
- [37] M. Shirayama, H. Kadowaki, T. Miyadera, T. Sugita, M. Tamakoshi, M. Kato, T. Fujiseki, D. Murata, S. Hara, T. N. Murakami, S. Fujimoto, M. Chikamatsu, H. Fujiwara, *Phys. Rev. Appl.* **2016**, *5*, 014012.
- [38] H. Li, C. Cui, X. Xu, S. Bian, C. Ngaojampa, P. Ruankham, A. P. Jaroenjittchai, *Sol. Energy* **2020**, *212*, 48.
- [39] B. Jin, D. Zhao, F. Liang, L. Liu, D. Liu, P. Wang, M. Qiu, *Research* **2021**, *2021*, 9797058.
- [40] Y. Shao, Z. Xiao, C. Bi, Y. Yuan, J. Huang, *Nat. Commun.* **2014**, *5*.
- [41] L. Zhang, P. H. L. Sit, *J. Phys. Chem. C* **2015**, *119*, 22370.
- [42] W. Kaiser, K. Hussain, A. Singh, A. A. Alothman, D. Meggiolaro, A. Gagliardi, E. Mosconi, F. De Angelis, *J. Mater. Chem. A* **2022**, *10*, 24854.
- [43] J. S. Park, J. Calbo, Y. K. Jung, L. D. Whalley, A. Walsh, *ACS Energy Lett.* **2019**, *4*, 1321.
- [44] D. Meggiolaro, E. Mosconi, F. De Angelis, *ACS Energy Lett.* **2019**, *4*, 779.
- [45] Z. Dang, J. Shamsi, F. Palazon, M. Imran, Q. A. Akkerman, S. Park, G. Bertoni, M. Prato, R. Brescia, L. Manna, *ACS Nano* **2017**, *11*, 2124.
- [46] Y. Ouyang, Y. Li, P. Zhu, Q. Li, Y. Gao, J. Tong, L. Shi, Q. Zhou, C. Ling, Q. Chen, Z. Deng, H. Tan, W. Deng, J. Wang, *J. Mater. Chem. A* **2019**, *7*, 2275.
- [47] A. J. Pearson, G. E. Eperon, P. E. Hopkinson, S. N. Habisreutinger, J. T. W. Wang, H. J. Snaith, N. C. Greenham, *Adv. Energy Mater.* **2016**, *6*, 1600014.
- [48] D. Bryant, N. Aristidou, S. Pont, I. Sanchez-Molina, T. Chotchunangatchaval, S. Wheeler, J. R. Durrant, S. A. Haque, *Energy Environ. Sci.* **2016**, *9*, 1655.
- [49] L. Zhang, P. H. L. Sit, *J. Mater. Chem. A* **2017**, *5*, 9042.
- [50] N. Aristidou, C. Eames, I. Sanchez-Molina, X. Bu, J. Kosco, M. Saiful Islam, S. A. Haque, *Nat. Commun.* **2017**, *8*, 15218.
- [51] S. K. Matta, C. Tang, A. P. O'Mullane, A. Du, S. P. Russo, *ACS Appl. Nano Mater.* **2022**, *5*, 14456.
- [52] D. Meggiolaro, E. Mosconi, F. de Angelis, *ACS Energy Lett.* **2017**, *2*, 2794.
- [53] J. P. Perdew, K. Burke, M. Ernzerhof, *Phys. Rev. Lett.* **1996**, *77*, 3865.
- [54] P. Giannozzi, S. Baroni, N. Bonini, M. Calandra, R. Car, C. Cavazzoni, D. Ceresoli, G. L. Chiarotti, M. Cococcioni, I. Dabo, A. Dal Corso, S. de Gironcoli, S. Fabris, G. Fratesi, R. Gebauer, U. Gerstmann, C. Gougousis, A. Kokalj, M. Lazzeri, L. Martin-Samos, N. Marzari, F. Mauri, R. Mazzarello, S. Paolini, A. Pasquarello, L. Paulatto, C. Sbraccia, S. , G. Sciauzero, A. P. Seitsonen, et al., *J. Phys.: Condens. Matter* **2009**, *21*, 395502.
- [55] S. Grimme, J. Antony, S. Ehrlich, H. Krieg, *J. Chem. Phys.* **2010**, *132*, 154104.
- [56] A. Poglitsch, D. Weber, *J. Chem. Phys.* **1987**, *87*, 6373.